Journal of Current Science and Technology

Journal homepage: https://jcst.rsu.ac.th

Automatic Melanoma Skin Cancer Detection and Segmentation using SnakeCut Algorithm

Dondapati Rajendra Dev[1,2,*], T. Sivaprakasam[1], K. Vijaya Kumar[3]

[1]Department of Computer Science & Engineering, Annamalai University, Annamalai Nagar, Tamil Nadu, India
[2]Department of Computer Science & Engineering, Vignan's Institute of Engineering for Women, Kapu Jaggaraju Peta, Vsez Post, Visakhapatnam, India
[3]Department of Computer Science & Engineering, Gitam University, Vishakhapatnam, Andhra Pradesh, India

*Corresponding author; E-mail: rajendra0511@gmail.com

Abstract

Early detection of melanoma skin cancer is crucial for effective treatment, and computer-aided diagnostic technologies offer promising advancements for dermatologists to make faster, more precise diagnoses of skin lesions. Segmenting skin lesions is a crucial first step towards automated Computer-Aided Diagnosis for skin cancer. This paper aims to use SnakeCut, a foreground extraction approach, to automatically segment skin lesions in HSV color space with little human interaction. Active contour (otherwise called Snake) and Improved GrabCut are the two popular methods. By decreasing the energy function of the related contour, the active contour acts as a deformable segmentation contour. Improved GrabCut uses updated iterated graph cuts to store color attributes used as segmentation signals in order to achieve foreground segmentation from close-by pixel similarities in its foreground segmentation algorithm. The proposed integrated solution, which is predicated on a probabilistic framework, is termed "SnakeCut." We removed the outer black border using preprocessing. Later feature extraction is done using HOG and HSV and classifies the benign or melanoma state using Naïve Bayes, Decision tree, and K-nearest neighbor classifiers. The efficiency of the segmentation strategy was measured using the Jaccard Index. We compared the classification results of our method with existing state-of-the-art approaches. The study demonstrates the efficacy of Automatic SnakeCut in accurately segmenting skin lesions, thereby enhancing the performance of subsequent classification tasks. The average F-score was 0.75 on the 2017 ISIC challenge training dataset of 100 images. Compared to other methods, this study's findings reveal that the suggested method is highly accurate.

Keywords: CAD Systems; Active Contour; GrabCut; SnakeCut; Object segmentation

1. Introduction

In recent days, computers and intelligent portable gadgets are already ubiquitous and can thus assist in the early detection of melanoma. It is possible to combine these technologies with CAD technology to create an intelligent system that aids dermatologists in the detection of malignant melanoma. Melanoma, the deadliest form of the disease, causes about 75% of all skin cancer fatalities (Titov et al., 2019; Siriwath et al., 2021). Early detection of melanoma improves survival rates, but manual diagnosis requires skilled specialists and results may vary among observers. To help pathologists work more accurately and efficiently, it's important to develop an accurate, dependable, automated melanoma detection system

(Takruri, & Abubakar, 2017). Automatic melanoma diagnosis from dermoscopy images, however, is still a laborious process because of many limitations. First, it is difficult to accurately segment lesions because of the weak contrast between lesions and normal skin. Second, there may be a considerable degree of visual resemblance between melanoma and non-melanoma lesions, making them challenging to recognize. Third, people with varied skin issues, such as different skin colors, hair types, or vein patterns, will have various melanoma appearances in terms of color, texture, and other features.

Traditional CAD algorithms for melanoma diagnosis rely on three steps: segmenting the lesion, extracting features, and classifying these features (Singh et al., 2017; Sayed et al., 2024). Segmentation is the splitting of an image into disjointed areas uniform in terms of features such as brightness, color, and texture. The purpose of segmentation is to make it easier to extract useful information from an image by simplifying its representation. Many comparative studies analyze the performance of various segmentation methods (Katapadi et al., 2018; Jaworek-Korjakowska, 2016). Once the lesion has been identified, relevant features are extracted using different chromatic and morphological parameters for categorization.

Skin lesion segmentation is usually the initial stage in classification procedures. Celebi et al. (2015) provided a recent analysis of automated skin lesion segmentation techniques. Accurate segmentation can lead to more effective lesion classification accuracy. Several research studies (Celebi et al., 2009; Iyatomi et al., 2008; Nagaoka et al., 2012; Celebi et al., 2007; Garnavi et al., 2010; Peng et al., 2009) have been conducted to obtain acceptable lesion segmentation outcomes. Despite all the work that has been done in terms of skin lesion segmentation and classification, more work needs to be done. Since 2016, the International Skin Imaging Collaboration's (ISIC) databases for autonomously analyzing skin lesions have been increasing progressively. Using the annotation-based datasets published at ISIC 2017 for lesion segmentation, dermoscopic feature extraction, and lesion classification, researchers can enhance the accuracy of automated melanoma detection systems. The work by Wang et al. (2018) focuses on the CV model's energy function, reconstructed by mixing HSV models, and the k-means method was used to pre-segment the algorithm to achieve

unsupervised segmentation. Full advantage was taken of color image information to address various color image segmentation challenges.

This paper deals with SnakeCut, a simple yet strong image segmentation algorithm, used to segment a skin lesion using the improved HSV color space and analyze the results. This SnakeCut technique uses active contours, or snakes, as flexible, deformable curves to outline object boundaries in images. Although it accurately delineates the boundaries of melanoma lesions, aiding in analysis and diagnosis. It also contributes to feature extraction, crucial for melanoma classification, and provides high-quality segmentation results, which are essential for subsequent classification algorithms. The results were validated using a publicly available dataset, ISIC 2017, containing RGB images of various resolutions normalized using the proposed method titled "SnakeCut" because it utilizes a probabilistic framework to combine the results of Snake and Improved GrabCut. The user is required to provide a rectangle or polygon enclosing the foreground object in SnakeCut (lesion) without requiring post-corrective editing.

1.1 Related Work

This section discusses some of the most common skin cancer diagnostic methods. The main aim of the SnakeCut approach is to focus on the automatic foreground extraction of skin lesions and their segmentation into HSV channels with very minimal human intervention. Early detection of melanoma skin cancer is crucial for effective treatment, and computer-aided diagnostic technologies offer promising advancements for dermatologists to make faster, more precise diagnoses of skin lesions.

Shan et al. (2020) presented the FC-DPN segmentation architecture to overcome these challenges, based on the Dual-Path Network (DPN) and Fully Convolutional Network (FCN). These techniques may effectively reuse and re-exploit existing features because of the DPN's residual and densely linked route advantages. There are two types of Sub-DPN blocks used in fully convolutional DenseNets, called FC-DenseNets. These sub-DPN blocks were used to replace dense blocks. FC-DPN now has more informative and discriminative features for better segmentation, according to this framework. The original dataset ISBI comprises inaccurate ground truth images, so, to rectify them,

they replaced it with the new ISBI 2017 dataset (i.e., the Skin Lesion Challenge dataset). The simulation results on the proposed system yield a Jaccard index of 80.02% on the PH2 dataset.

Ding et al. (2021) used MobileNetV3-U-Net, a lightweight encoder-decoder, to conduct automatic SLS while utilizing minimal resources. Semantic segmentation requires encoder-decoder architecture, learning algorithms, and post-processing methods. They changed the decoder to use the BCDU-bidirectional Net's ConvLSTM layer and separable-UNet blocks to improve SLS. They randomly added images to the training dataset to avoid overfitting. Averaging several local optima using stochastic weight averaging (SWA) learning increased generalization. They used three publicly accessible datasets to test their method: ISIC-2017, ISIC-2018, and PH2. Tests conducted on this model have shown that it outperforms various other leading-edge approaches.

Wei et al. (2019) discussed how computer-aided diagnosis (CAD) of skin cancer relies heavily on accurate, automatic identification of skin lesions. They presented a new method for automatically segmenting skin lesions to get an exact border. Otsu's threshold is used to remove the initial lesion. The second phase involves inspecting the surroundings. To separate small homogeneous sub-regions, Simple Linear Iterative Clustering (SLIC) is used, followed by supervised learning to classify them as background skin or lesion, resulting in an accuracy borderline. The suggested technique outperforms four existing modern automated segmentation techniques in a series of tests.

das Chagas et al. (2020) and Wibowo et al. (2021) showed how time and efficiency can be balanced. To automatically separate skin lesions based on probabilistic features, the Parzen window (SPPW) was used. The PH2 and ISIC datasets were used to obtain the method's findings. Based on these two datasets, the SPPW approach produced average results of 98.55% in terms of specificity, accuracy, Dice, and sensitivity, as well as a Jaccard Index score of 88.45%. Two of the method's best points are its quick average segmentation time per image and metric values that are often higher than those achieved by competing methods. The SPPW segmentation approach provides dermatologists an easy-to-use, rapid way to classify diseased skin.

Wibowo et al. (2021) showed that a significant number of parameters and FLOPs are required to achieve good skin lesion segmentation performance using deep learning models, which limit the situations in which they may be used. Feature maps at the low level, which are crucial for accurately predicting certain pieces of information, should be more utilized in these models. They presented EUnet-DGF, a lightweight encoder that employs MBconv and boasts high encoding capability. They predicted pixels on small patterns using an insight-gated fusion block that combines image features from different depths and improves prediction accuracy. The proposed model performs well when tested against datasets from ISIC 2017 and PH2. In terms of parameters and FLOPs, EUnet-DGF constitutes only a small fraction of Unet's initial size.

das Chagas et al. (2020) utilized a topology known as a multi-swarm, which segregates the population into several smaller swarms. This approach was implemented using the multi-swarm coyote optimization algorithm (MCOA) to assess its efficacy across various benchmark functions. Additionally, they investigated a multi-level thresholding issue with 44 images from the PH2 benchmark dataset of skin dermoscopic data to gauge its effectiveness. The findings indicate that a multi-swarm architecture enhances the diversity of the population and consequently, the exploration capability. Compared to traditional methods and other advanced meta-heuristic optimization techniques, the results demonstrate that MCOA is both more stable and accurate. MCOA is also being applied to develop a new segmentation model for skin lesions. The results suggest that, in the future, the detection and treatment of skin diseases could be significantly facilitated by this method.

2. Objective

The primary goal of the proposed research is to develop a machine learning architecture specifically designed for the segmentation of skin cancer lesions. Central to this endeavor is the SnakeCut approach, which emphasizes automated foreground extraction of skin lesions segmented into HSV channels, requiring minimal human intervention. Early detection of melanoma, a serious form of skin cancer, is vital for effective treatment. Consequently, advancements in computer-aided diagnostic technologies are increasingly essential, providing dermatologists with the tools to make quicker and more accurate diagnoses of skin lesions.

3. Materials and methods

The proposed work was automatically executed with minimal human intervention, employing a modified version of the GrabCut algorithm. Figure 1 illustrates the workflow of the segmentation pipeline. This pipeline begins by taking a preprocessed image as input. Subsequently, the pixels are clustered using the enhanced "k-means clustering," and the BGR image is converted to HSV. Adaptive thresholding is then applied to derive a probable lesion mask from the image. Following this, a thresholding approach is utilized to determine whether to apply a mask for SnakeCut Segmentation.

3.1 Dataset description:

The dataset utilized for this study was sourced from the ISIC 2017 Challenge, organized by the International Skin Imaging Collaboration. To access the dataset, one can visit the following URL on the ISIC website: https://challenge.isic-archive.com/data/. This dataset is often employed to train and evaluate machine learning models for the detection and classification of skin cancer, representing the largest publicly accessible collection of dermoscopy images. It comprises 2,000 ground-truth images for training purposes, 150 segmented images for validation, and 600 images for testing—none of which include ground-truth labels. However, all images provide patient identifiers, sex, ages, and basic anatomical sites. Figure 2 illustrates various examples of skin lesions associated with melanoma.

3.2 Preprocessing

The preprocessing step is designed to correct image defects that occur during the acquisition process by removing various artifacts, such as hair and ruler lines, which may compromise the accuracy of segmentation and lead to incorrect classifications. Ideally, the acquired image should be free of these aberrations; however, removing hair presents challenges due to its complexity. To address this, an adaptive median filter is employed to smooth out the replaced hair pixels. This technique is also used to eliminate dark frames surrounding small images. In Figure 3, the handling of these preprocessing steps is demonstrated. Based on the pixel values in the dark areas, a mask is generated for each image. This mask is then utilized to inpaint the neighboring pixels within the black border area, ensuring a cleaner image presentation for subsequent analysis.
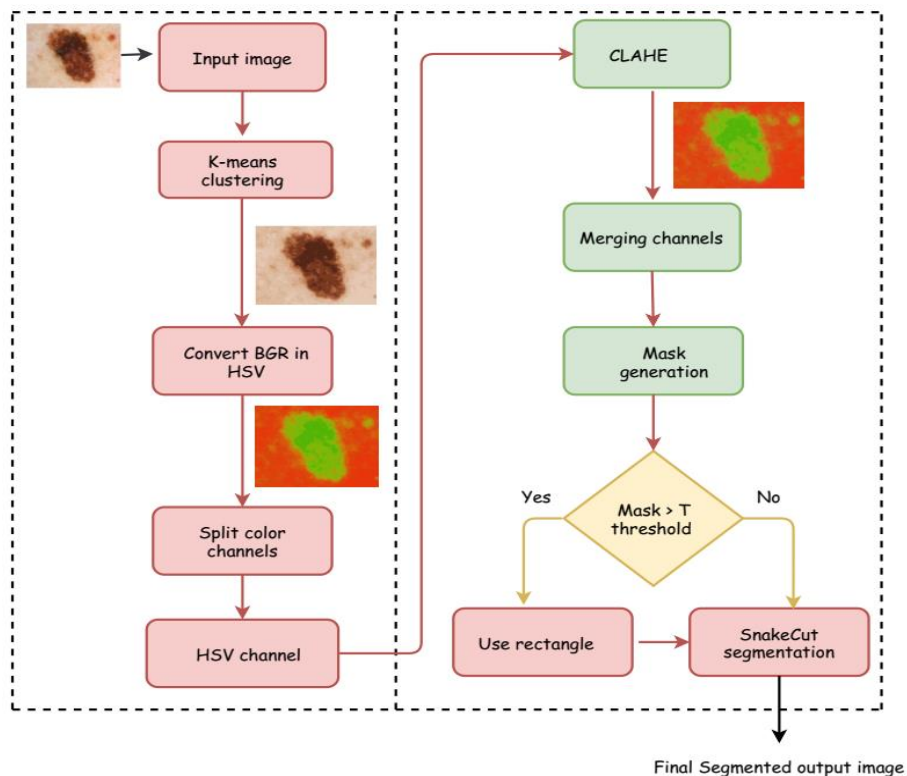
Figure 1 Proposed scheme's block diagram

3.3 Color Quantification

K-means clustering was employed to achieve color quantization. Subsequently, the image was converted from BGR to HSV color space. Each channel was then separated and subjected to adaptive histogram equalization independently. Following this, all the color channels were merged, as illustrated in Figure 4.

Figure 2 Sample Images from ISIC 2017 dataset
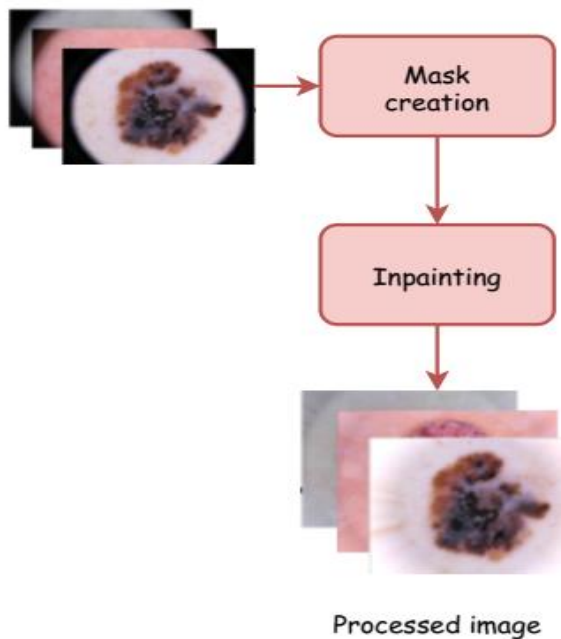
Figure 3 Dark outer border removal pipeline
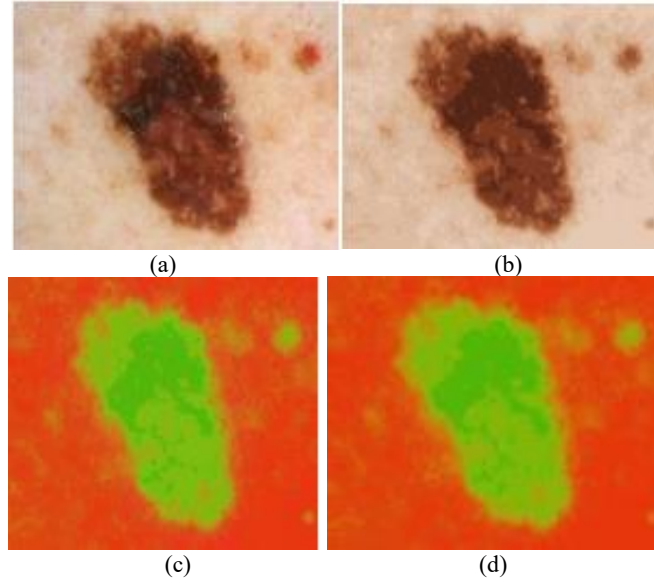
Figure 4 a) The original image b) k-means clustering c) RGB to HSV d) Adaptive Histogram Equalization

3.4 Contrast Limited Adaptive Histogram Equalization (CLAHE)

CLAHE (Contrast Limited Adaptive Histogram Equalization) concentrates on tiles that function as small fragments of an image (T. O. Sunitha et al., 2022). To eliminate false borders, neighboring tiles are merged using "bilinear interpolation." This method can also be applied to color images, typically utilizing the luminance channel. When only the brightness channel of an HSV image is equalized, the results are significantly superior compared to equalizing all the channels of a BGR image.

3.5 Lesion/image segmentation

The classification of a skin lesion commences with segmentation. A robust segmentation method is crucial for identifying diseased regions with higher accuracy and addressing various challenges such as color variations, the presence of hair, and lesion irregularity. After adjusting the images to maintain a consistent aspect ratio, the segmentation process is completed in two sequential steps:

1) Contrast stretching is employed to distinguish the lesion (foreground) region from the background.
2) The SnakeCut-based segmentation approach is used to segment the lesion region.

3.6 Active Contour (Snake) Model

In this model, one of the important forms is the parametric curve shown symbolically as $v(s) =$ $[x(s), y(s)]$, where's belongs to $\{0, 1\}$ that minimizes with below energy function.

$$E_{snake} = \int_0^1 \frac{1}{2}\left(\eta_1|v'(s)|^2 + \eta_2|v''(s)|^2\right) + E_{ext}\left(v(s)\right)ds \quad (1)$$

We use the weighting constants η_1 and η_2 to assess the relative importance of the material's elastic and bending properties. The terms $v'(s)$ and $v''(s)$ represent are 1st and 2nd "order derivatives" of $v(s)$, respectively. We constructed E_{ext} from the image to capture smaller values at features of interest such as edges and object boundaries. The normal external energy required to move a snake towards step edges in an image $I(x, y)$, where (x, y) are spatial coordinates, is defined as follows (Mei et al., 2016).

$$E_{ext} = -\left|\nabla I(x, y)\right|^2 \quad (2)$$

In color images, the intensity gradient is calculated using the gradient operator ∇. This is achieved by summing the gradients of the R (red), G (green), and B (blue) bands at each pixel, as shown in Eq. 3. The resulting composite gradient highlights the overall intensity variation across all three-color channels, providing a comprehensive measure of edge strength and direction at each point in the image.

$$|\nabla I| = \max\left(|\nabla R|, |\nabla G|, |\nabla B|\right) \tag{3}$$

Eq. 3 generates a gradient that yields superior edge information. Accordingly, a snake that aims to minimize E_{snake}, must satisfy the Euler equation, as referenced in Mei et al. (2016).

$$\eta_1 v''(s) - \eta_1 v''''(s) - \nabla E_{est} = 0 \tag{4}$$

In equation (4), $v''(s)$ represents the second-order derivative, and $v''''(s)$ represents the fourth-order derivative of $v(s)$. This formula is part of what is known as an active contour model, or "snake," in certain fields. The active contour model is an energy-minimizing spline influenced by external constraint forces and image forces, which draw it towards features such as edges and lines. The term "snake" derives from its behavior, as it clings to neighboring edges and accurately captures their location. The interaction of both external and internal forces determines the contour's behavior in dynamic situations, as described by the equation below.

$$\xi v_t = F_{\text{int}} + F_{ext} \tag{5}$$

where ξ is a non-negative arbitrary constant and v_t is the partial derivative of v with respect to t. As the deforming contour nears the object boundary, the total influence from the two forces—internal and external—equates to zero, causing the contour to come to a halt. This equilibrium point is critical, as it indicates that the contour has optimally aligned with the boundary of the object, fulfilling the primary goal of the active contour model.

GrabCut: In the GrabCut algorithm, the user is first required to select an "area of interest" before the segmentation of a foreground object begins. Consider the image I as a pixel array indexed by a single single index, n.

$$z = (z_1, ..., z_n, ..., z_N) \tag{6}$$

where z_n is represented in RGB color space. The segmentation of the image is depicted by an array of "opacity" values at each pixel.

$$\alpha = (\alpha_1, ..., \alpha_n, ..., \alpha_N) \tag{7}$$

In "hard segmentation," the α_n typically ranges between 0 and 1, where 0 denotes the background and 1 denotes the foreground. GrabCut utilizes two independent Gaussian mixture models (GMMs) to represent the color distributions of these segments. Each GMM is a K-component model with full covariance—one for the foreground and one for the background. When integrating with the resilience of the GMM in an optimization model, it is necessary to incorporate $k = (k_1,..., k_n,..., k_N)$, by each k_n $1,..., K$ representing one of the K components. Each pixel is assigned to a single GMM component, determined by whether α_n is equal to zero (background) or one (foreground). This assignment significantly influences the model's ability to accurately segment the image based on the defined foreground and background distributions.

3.7 Improved Grapcut

In the improved GrabCut approach, we employed two methods along with a single threshold value to enhance segmentation. The process initiates with a mask of the lesion location. If the mask's extracted value surpasses the threshold, a rectangle is generated for the GrabCut algorithm.

3.8 Proposed Snakecut: Hybrid Active Contour and Improved GrabCut

Active contour utilizes an intensity gradient to construct a contour around the user's input or within the item, facilitating the precise determination of its borders. Conversely, GrabCut segments pixels based on their color distribution and incorporates global cues, allowing it to effectively remove irrelevant parts (such as background elements) from within the object border. For segmentation, these two algorithms leverage complementary data, including region-based and edge-based information. In this paper, we describe an integrated strategy, termed SnakeCut, which combines these complementary approaches for enhanced object segmentation. Figure 5 illustrates the overall flow diagram of the segmentation method. SnakeCut autonomously employs both Active Contour and GrabCut to segment the input image.

We integrated the two segmentation results using SnakeCut's probabilistic architecture. By applying probabilistic criteria, we synthesized the final segmentation result from these two inputs. Algorithm 1 outlines the principal steps of the SnakeCut algorithm. Implementing a probabilistic

framework was essential to merge the two results effectively. Within this framework, C0 (the active contour) identifies the object boundary, and each pixel z_i is assigned two probabilities: $Ps(zi)$ and $Pc(zi)$. $Ps(zi)$ the pixel's proximity to the border, whereas $Pc(zi)$ assesses the pixel's similarity to the background. A high value for $Ps(zi)$ suggests that pixel $Ps(zi)$ is distant from the border, while a high value for $Pc(zi)$ indicates that the pixel closely resembles the background. To decide whether a pixel belongs in the foreground or background, we employ the decision function p.

$$p(z_i) = \rho P_c(z_i) + (1-\rho) P_s(z_i) \qquad (8)$$

In Equation (8), ρ denotes empirically learned weight that determines relevance of two strategies. The probability P_c was calculated using distance transform (DT) of that object boundary C_0. It can be calculated using the following formula:

$$I_d(z_i) = \begin{cases} 0, if \ z_i \ \text{lies on contour } C_0 \\ d, \text{otherwise} \end{cases} \qquad (9)$$

Here d denotes the Euclidian distance among both pixel z_i and the nearest contour point in equation (9), and before approximating P_c, distance transform data are normalized in [0, 1]. In is the "normalized distance transform image", and d_n is the transform value of pixel z_i in I_d.

To predict the probability P_c of z_i, the following fuzzy distribution function is used:

$$P_c(z_i) = \begin{cases} 0, & 0 \le d_n < a; \\ 2\left(\dfrac{d_n - a}{b - a}\right)^2, & a \le d_n < \dfrac{a+b}{2}; \\ 1 - 2\left(\dfrac{b - d_n}{b - a}\right)^2, & \dfrac{a+b}{2} \le d_n < b; \\ 1, & b \le d_n \le 1. \end{cases} \qquad (10)$$

In equation (10), a and b are constants for $a < b$. Thus, it results in a piecewise constant function having a transition from 0 to 1 at $(a + b)/2$ when $a \ge b$. We adjusted the probability distribution function to have a small probability value *of Pc* near

contour *C0* and a large probability value *of Pc* for points farther away. The nonlinear behavior of this fuzzy function is determined by these two values (a, b). By varying the parameters a and b, we can influence the nonlinear behavior of this fuzzy function. To evaluate the output response of Snake, parameters a and b must be defined first, followed by defining the parameter of GrabCut as a second step.

Algorithm 1: SnakeCut Steps
Input: RGB Image I
Output: I_{sc}.
In I_{sc}, we set all the pixels to 0.
begin
Segmentation process
1. Using Active Contour, the primary purpose is to ensure desired object segmentation in image I.
2. Assume that the contour's object boundary is C_0 and "Active Contour" is I_{ac}.
3. Using GrabCut, segment the appropriate object in I.
4. Assuming that the output is I_{gc}.
B. Process of amalgamation of SnakeCut
1. Locate a group of pixels Z in image I that fall under contour C_0.
2. Consider for every pixel $z_i \in Z$,
    (a) By Eq. 10, **do** computation for $p(z_i)$
    (b) **if** $p(z_i) \le T$, **then**
    $I_{sc}(z_i) = I_{ac}(zi)$
    else
    $I_{sc}(z_i) = I_{gc}(z_i)$
end if
By carefully selecting values for a and b, we can effectively regulate the size of points deemed to be near the contour. P_c is set to 0 when a pixel's distance from the border is within the range $[0, a]$, and 1 when the distance spans $[b,1]$. All values have been standardized to maintain consistency. As illustrated in Figure 1, the region of interest undergoes segmentation. This segmented area is then leveraged to extract features, which are subsequently employed by classifiers to assess whether the image indicates the presence of melanoma or a benign condition. The methodology for feature extraction and classification is detailed in Figure 6, outlining each step involved in the process.
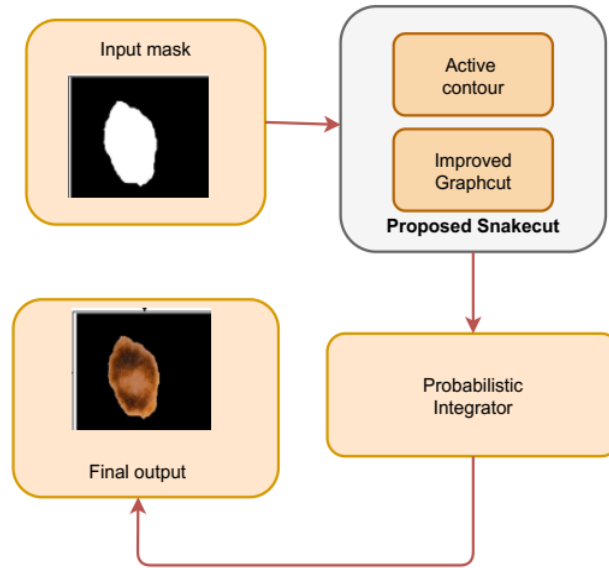
Figure 5 The proposed SnakeCut technique's flow chart
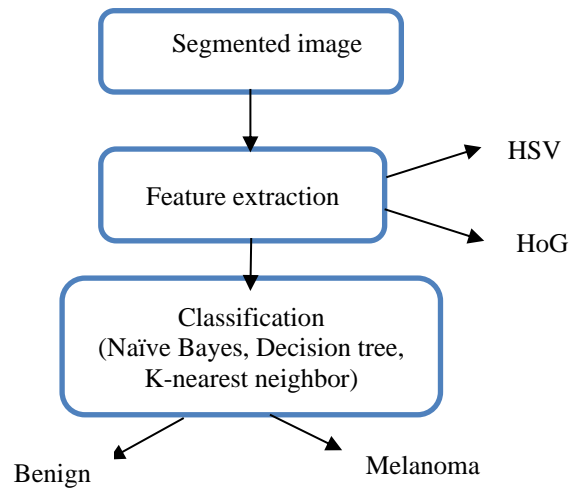
Figure 6 Feature extraction and classification methodology

3.9 Feature extraction

The detection of melanoma skin cancer heavily relies on color features, which significantly influence the performance of the utilized framework. This is achieved by resampling the RGB image into HSV and YCbCr color spaces from their individual channels. Images within these color spaces are then processed to extract distinct features. The HSV (Hue, Saturation, Value) color space is complementary to RGB. In HSV, Hue represents the spectrum of colors available, Saturation indicates the percentage of grey, and

Value describes the intensity of a color, reflecting the color's brightness and tint. In contrast, the YCbCr color space consists of three components: Y for brightness, Cb for chrominance, and Cr for saturation. From each channel of these color spaces, four statistical measures are extracted: mean, standard deviation, skewness, and entropy. For instance, in the HSV color space, four features are extracted from the Hue channel, four from the Saturation channel, and four from the Value channel, resulting in a total of 12 features from a single-color space. Subsequently, a 24-element

feature vector is constructed by combining the feature vectors from both HSV and YCbCr color spaces. This comprehensive approach facilitates robust analysis, enhancing the accuracy of melanoma detection.

Color features play a crucial role in determining whether a tumor is cancerous or benign, as doctors often rely on these characteristics for quick analysis, despite geometric variations in lesion structures. Three primary color spaces—RGB, HSI, and LAB—are used to extract these features. For each channel in these color spaces, statistical measures such as mean, standard deviation, skewness, and kurtosis are computed.

HOG features, also known as shape-based features, focus on the form of objects. In our study, we extract HOG features from the shapes of segmented skin lesions, enabling effective performance. The ISIC institutional database, a public repository containing 1022 x 1022 RGB dermoscopic images of high quality, is frequently used in skin cancer research. Although ISIC encompasses a wide array of data, for our purposes, we accessed 290 images, comprising 130 melanoma and 160 benign cases. We conducted tests on multiple features, including color and HOG features, to verify the efficacy of the proposed approach. Additionally, we evaluated three different types of classification systems.

Classification involves categorizing images as either benign or malignant using classifiers. In this research, we rigorously tested the system using three distinct classifiers to ensure robustness and accuracy in our findings.

Naïve Bayes: Naïve Bayes is a classification technique grounded in Bayes' Theorem, utilizing probability calculations to make classifications. In our analysis, we rigorously tested the system by experimenting with various parameters that affect the operation of the function.

Decision tree: Decision tree classification involves categorizing information by splitting it into multiple groups with similar characteristics. The accuracy of a decision tree is influenced by the maximum number of splits allowed and the criteria for establishing a split. These factors are carefully adjusted to optimize the tree's performance.

K-nearest neighbors (KNN): K-nearest neighbors (KNN) is another classification technique employed in our study. In this method, new instances are classified based on similarity measures derived from the nearest neighbors. These

neighbors are identified during the training phase, where the features vector and their corresponding labels are stored. The validity of KNN, compared to other methods, is confirmed by a confusion matrix which demonstrates its classification accuracy on the ISIC 2017 dataset.

To assess the system's efficiency, three performance measures are utilized, and each is evaluated independently. The determination of these metrics involved the use of four parameters: TP (True Positive), TN (True Negative), FP (False Positive), and FN (False Negative). The labeled test set (y) and predicted labels (y1) are critical in calculating these values, ensuring an accurate evaluation of classifier performance.

$$\text{Sensitivity (Sen)} = \frac{TP}{TP + TN} \tag{11}$$

$$\text{Specificity (Spec)} = \frac{TN}{TN + FP} \tag{12}$$

$$\text{Accuracy (Acc)} = \frac{TP + TN}{TP + FP + FN + TN} \tag{13}$$

$$\text{Jaccard Coefficient (JC)} = \frac{|y \cap y1|}{|y \cup y1|} \tag{14}$$

4. Results and discussion
4.1 Results

All simulations discussed in this paper were conducted using Jupyter Notebook to explore skin lesion segmentation with the Automatic SnakeCut technique. The proposed approach was assessed using the publicly available ISIC Challenge 2017 dataset. Performance measures were employed to demonstrate the efficiency of the framework. The system underwent training and testing through five-fold cross-validation. The segmentation method was tested on 100 images from the ISIC Challenge 2017 dataset, achieving an average Jaccard Coefficient (JC) of 0.71. The performance of the proposed pipeline, as indicated in Table 1, includes some segmentation. Variability in skin characteristics, such as wrinkles, means that dermoscopic image collections may contain numerous microscopic objects. The median filter is employed to eliminate objects that are too small to be relevant, although not all impurities are removed completely. This partial removal can impact the performance and outcomes of the algorithm. Table 2 presents several performance parameters for five images randomly selected from the ISIC Challenge 2017 dataset. To assess the performance of the

proposed work relative to existing methods, a set of widely accepted statistical evaluation metrics was utilized. The proposed technique underwent testing on 100 skin images from the ISIC dataset, which included both benign and melanoma lesions, ensuring a comprehensive evaluation.

Figure 7 presents a list of segmentation results, with measurements sourced from original articles to evaluate the efficiency of each comparative approach. The proposed method achieves superior results compared to those described by Yuan et al. (2017), Al-masni et al. (2018), and Guo et al. (2018). It yields the highest

values for sensitivity (98.2%), demonstrating its ability to effectively detect true positive cases of melanoma and minimize false negatives. Its specificity (98.9%) indicates that the system can accurately differentiate between benign and malignant lesions, reducing false positives. Additionally, an accuracy of 96.3% in melanoma detection suggests that the system can reliably distinguish between benign and malignant lesions. The high metrics underscore the system's efficiency in detecting melanoma, enhancing early detection, accurate diagnosis, and improved patient outcomes.

Table 1 Qualitative and Quantitative results of segmentation

Original Image	Ground Truth	Segmented Image	JC
			0.68
			0.87
			0.78
			0.85
			0.75
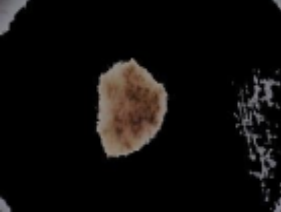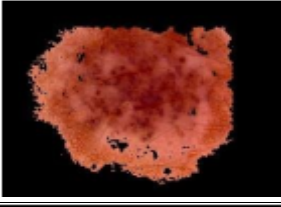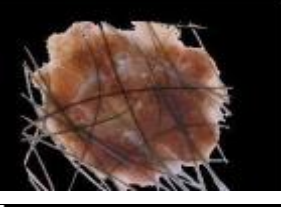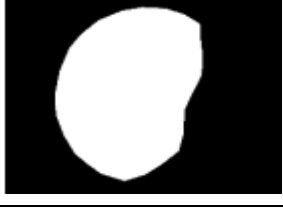
Table 2 Comparison of proposed work with existed works on ISIC 2017 database

Authors	Sensitivity in %	Specificity in %	Accuracy in %
(Yuan et al. 2017)	82.5	97.5	93.4
(Al-masni et al. 2018)	85.4	96.69	94.03
(Guo et al. 2018)	97.5	88.8	95.3
Our work	**98.2**	**98.9**	**96.3**
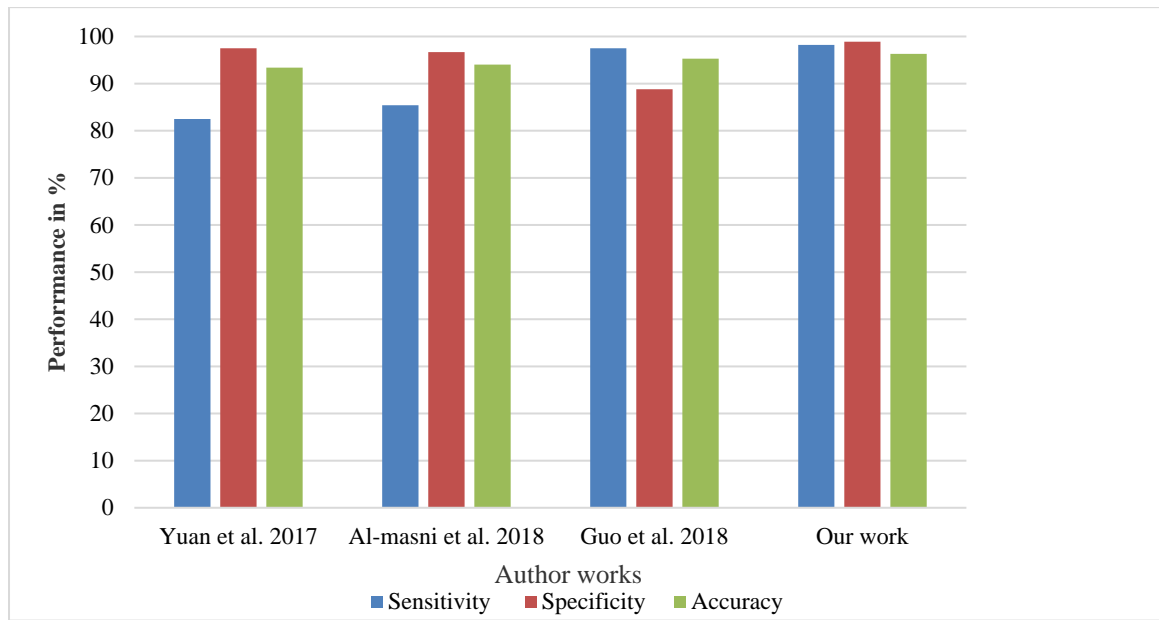
Figure 7 Performance comparison of three evaluation metrics of existed works and proposed work on ISIC 2017 database
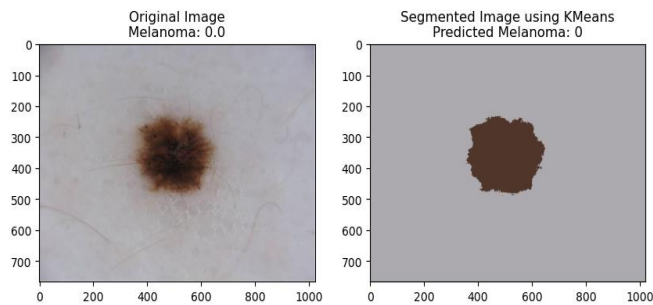
Figure 8 K-Means Clustering

The proposed approach demonstrates superior performance, outperforming related methods in segmenting skin lesions. The study significantly surpasses approaches used by other researchers with the ISIC 2017 database in terms of sensitivity, specificity, and accuracy. Figure 8 displays the results of K-Means Clustering, illustrating both the original and the segmented images.

Figure 9 The BGR2 HSV result in which it shows the original, inpainted, segmented, and HSV images respectively.

Table 3 presents the results of various feature sets, highlighting that the basic classifier, Decision Tree (DT), performs well in comparison to other approaches. Figure 10 illustrates the preprocessing results using CLAHE, showcasing all the color channels.
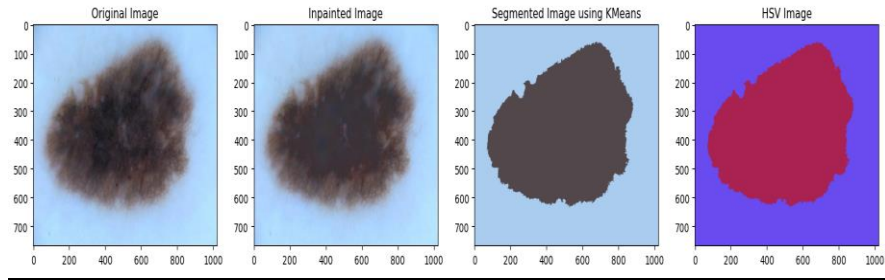
Figure 9 BGR2 HSV

Table 3 Results for individual extracted set of features using ISIC-2017 dataset

Classifier	Selected features		Performance measures			
	Color	Hog	Sen	Prec	Spec	Acc
NB	√		89.4	89.65	91.9	89.7
		√	90.1	91.2	91.9	90.2
KNN	√		88.3	88.12	89.3	88.3
		√	89.4	90.2	90.3	89.6
DT	√		91.5	91.6	92.3	90.9
		√	92.3	92.6	92.7	92.3
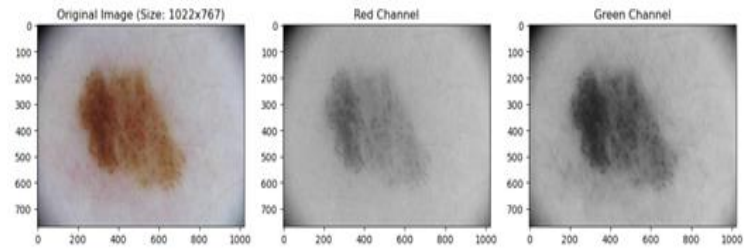
(a)
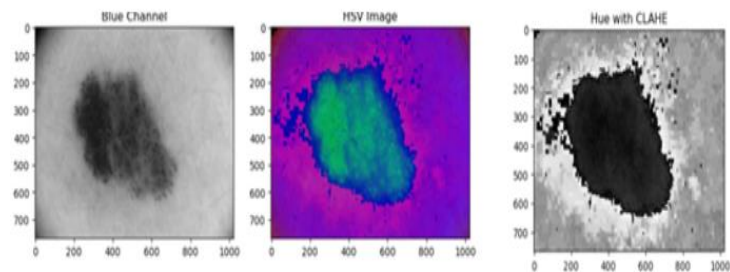
(b)
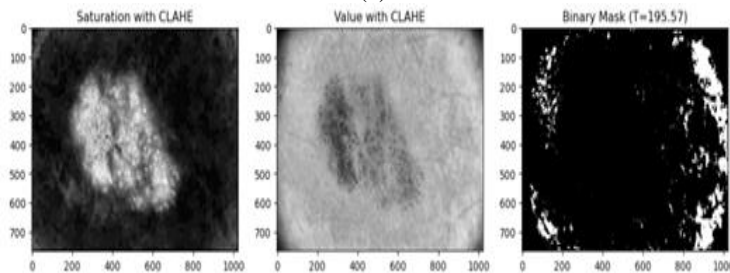
(c)

Figure 10 Preprocessing using CLAHE

Table 4 Confusion matrix for ISIC 2017 dataset

Class	Classification class		TPR (%)	FNR (%)
	Benign	Melanoma		
Benign	**91**	9	91	9
Melanoma	14	**86**	86	14

Data in bold are significant.

Table 4 displays the results of the confusion matrix for the ISIC 2017 dataset, indicating that the benign class has 91 instances while the melanoma class contains 86 instances.

4.2 Discussion

This paper introduces a SnakeCut-based segmentation framework designed to tackle the challenges of automated melanoma classification in dermoscopy images. The proposed framework consists of three interconnected steps: Segmentation, Feature Extraction, and Classification, which operate seamlessly without requiring manual intervention. Initially, the lesion region is segmented using the SnakeCut algorithm, which leverages machine learning techniques. Subsequently, a variety of color, texture, and shape features are extracted from the segmented images employing HSV and HOG methods. These features are then input into DT, NB, and KNN classifiers. Among these, the DT classifier yields the most favorable outcomes in terms of accuracy, precision, and specificity scores. This experiment was carried out using the open challenge dataset from the Skin Lesion Analysis toward Melanoma Detection on ISIC 2017. The findings suggest that the proposed melanoma classification system could integrate into a broader framework for skin lesion analysis. In the future, this approach might be expanded to enhance accuracy further by incorporating deep learning techniques for both segmentation and classification.

5. Conclusion

When the color distribution of certain foreground objects closely resembles that of the background, GrabCut alone tends to yield suboptimal segmentation results. In response, this paper introduces an automatic skin lesion segmentation framework employing the SnakeCut algorithm. The segmentation process is automated and generalized using auto-extracting masks and rectangle initialization procedures, simplifying the user's task to merely drawing a rectangle around the foreground object of interest. This approach leverages a probabilistic framework to automate object segmentation effectively. The proposed method is adept at preserving parts of the object that share the background's color and removing internal inconsistencies within the object. Furthermore, evaluation using the ISIC-2017 dataset demonstrates that the decision tree classifier excels, achieving a sensitivity of 92.3%, precision of 92.6%, specificity of 92.7%, and accuracy of 92.3%, outperforming both KNN and NB classifiers.

6. Acknowledgements

7. References

Al-Masni, M. A., Al-Antari, M. A., Choi, M. T., Han, S. M., & Kim, T. S. (2018). Skin lesion segmentation in dermoscopy images via deep full resolution convolutional networks. *Computer Methods and Programs in Biomedicine*, *162*, 221-231. https://doi.org/10.1016/j.cmpb.2018.05.027

Celebi, M. E., Iyatomi, H., Schaefer, G., & Stoecker, W. V. (2009). Lesion border detection in dermoscopy images. *Computerized Medical Imaging and Graphics*, *33*(2), 148-153. https://doi.org/10.1016/j.compmedimag.2008.11.002

Celebi, M. E., Kingravi, H. A., Iyatomi, H., Lee, J., Aslandogan, Y. A., Van Stoecker, W., ... & Marghoob, A. A. (2007, March 26). *Fast and accurate border detection in dermoscopy images using statistical region merging* [Conference Presentation]. Medical Imaging 2007: Image Processing, San Diego, CA, United States. https://doi.org/10.1117/12.709073

Celebi, M. E., Wen, Q. U. A. N., Iyatomi, H. I. T. O. S. H. I., Shimizu, K. O. U. H. E. I., Zhou, H., & Schaefer, G. (2015). A state-of-the-art survey on lesion border detection in dermoscopy images. *Dermoscopy Image*

Analysis, *10*(1), 97-129.
https://doi.org/10.1201/b19107-5

das Chagas, J. V. S., Ivo, R. F., Guimarães, M. T., Rodrigues, D. D. A., Rebouças, E. D. S., & Rebouças Filho, P. P. (2020). Fast fully automatic skin lesions segmentation probabilistic with Parzen window. *Computerized Medical Imaging and Graphics*, *85*, Article 101774. https://doi.org/10.1016/j.compmedimag.2020.101774

Ding, X., & Wang, S. (2021). Efficient Unet with depth-aware gated fusion for automatic skin lesion segmentation. *Journal of Intelligent & Fuzzy Systems*, *40*(5), 9963-9975. https://doi.org/10.3233/JIFS-202566

Garnavi, R., Aldeen, M., Celebi, M. E., Varigos, G., & Finch, S. (2011). Border detection in dermoscopy images using hybrid thresholding on optimized color channels. *Computerized Medical Imaging and Graphics*, *35*(2), 105-115. https://doi.org/10.1016/j.compmedimag.2010.08.001

Iyatomi, H., Celebi, M. E., Oka, H., & Tanaka, M. (2008, August 20-25). *An Internet-based melanoma screening system with acral volar lesion support* [Conference Presentation]. 2008 30th Annual International Conference of the IEEE Engineering in Medicine and Biology Society. Vancouver, BC, Canada. https://doi.org/10.1109/IEMBS.2008.4650375

Jaworek-Korjakowska, J. (2016). Computer-aided diagnosis of micro-malignant melanoma lesions applying support vector machines. *BioMed Research International*, *2016*, Article 4381972. https://doi.org/10.1155/2016/4381972

Katapadi, A. B., Celebi, M. E., Trotter, S. C., & Gurcan, M. N. (2018). Evolving strategies for the development and evaluation of a computerised melanoma image analysis system. *Computer Methods in Biomechanics and Biomedical Engineering: Imaging & Visualization*, *6*(4), 465-472. https://doi.org/10.1080/21681163.2016.1277785

Mei, Z., Hua, W. J., & Xing, P. X. (2016). Segmentation for range image based on snake active contour model. *International*

Journal of Signal Processing, Image Processing and Pattern Recognition, *9*(8), 393-400. https://doi.org/10.14257/ijsip.2016.9.8.33

Nagaoka, T., Nakamura, A., Kiyohara, Y., & Sota, T. (2012, August 28). *Melanoma screening system using hyperspectral imager attached to imaging fiberscope* [Conference Presentation]. 2012 Annual International Conference of the IEEE Engineering in Medicine and Biology Society, San Diego, CA, USA. https://doi.org/10.1109/EMBC.2012.6346777

Peng, Y., Wang, N., Wang, Y., & Wang, M. (2019). Segmentation of dermoscopy image using adversarial networks. *Multimedia Tools and Applications*, *78*, 10965-10981. https://doi.org/10.1007/s11042-018-6523-2

Sayed, G. I., Khoriba, G., & Haggag, M. H. (2020). The novel multi-swarm coyote optimization algorithm for automatic skin lesion segmentation. *Evolutionary Intelligence*, *17*, 679–711. https://doi.org/10.1007/s12065-020-00450-4

Shan, P., Wang, Y., Fu, C., Song, W., & Chen, J. (2020). Automatic skin lesion segmentation based on FC-DPN. *Computers in Biology and Medicine*, *123*, Article 103762. https://doi.org/10.1016/j.compbiomed.2020.103762

Siriwath, J., Wiriyakulsit, N., Klomkleang, P., Inpad, C., Roytrakul, S., &Kaewkong, W. (2021). SPHINX31 suppresses splicing factor phosphorylation and inhibits melanoma cell growth and aggressiveness. *Journal of Current Science and Technology, 11*(3), 346-354. https://doi.org/10.14456/jcst.2021.35

Singh, A., Maurya, R., Yadav, R., & Srivastava, V. (2017). Innovative Technique of Segmentation and Feature Extraction for Melanoma Detection. *International Journal of Computer Sciences and Engineering*, 5(10), 100-104. https://doi.org/10.26438/ijcse/v5i10.100104

Sunitha, T. O., Rajalakshmi, R., & Sujatha, S. S. (2022). Fuzzy based dynamic histogram equalization for enhancing quality of registered medical image. *Journal of Current Science and Technology, 12*(2), 243-264.

Takruri, M., & Abubakar, A. (2017, November 21-23). *Bayesian decision fusion for enhancing melanoma recognition accuracy* [Conference Presentation]. 2017 International Conference on Electrical and Computing Technologies and Applications (ICECTA), Ras Al Khaimah, United Arab Emirates. https://doi.org/10.1109/ICECTA.2017.8252063

Titov, K. S., Stepanova, V. V., Krasnorutskiy, A. V., & Nagaeva, M. V. (2019). Rare forms of skin cancer. *Russian Journal of Clinical Dermatology and Venereology*, *18*(6), 735–741. https://doi.org/10.17116/klinderma201918061735

Wang, L., Wang, S., Liao, Y., Ye, X., & Wang, T. (2018, August 5-8). Improved level set model for color image segmentation [Conference presentation]. 2018 IEEE International Conference on Mechatronics and Automation (ICMA). Changchun, China. https://doi.org/10.1109/ICMA.2018.8484379

Wei, Z., Guo, B., Li, C., & Chen, Z. (2019, November 28-30). *Speeded-up Simple Linear Iterative Clustering Based on Region Homogeneity* [Conference Presentation]. 2019 2nd International Conference on Safety Produce Informatization (IICSPI), Chongqing, China. https://doi.org/10.1109/IICSPI48186.2019.9096051

Wibowo, A., Purnama, S. R., Wirawan, P. W., & Rasyidi, H. (2021). Lightweight encoder-decoder model for automatic skin lesion segmentation. *Informatics in Medicine Unlocked*, *25*, Article 100640. https://doi.org/10.1016/j.imu.2021.100640

Yuan, Y., Chao, M., & Lo, Y. C. (2017). Automatic skin lesion segmentation using deep fully convolutional networks with jaccard distance. *IEEE Transactions on Medical Imaging*, *36*(9), 1876-1886. https://doi.org/10.1109/TMI.2017.2695227